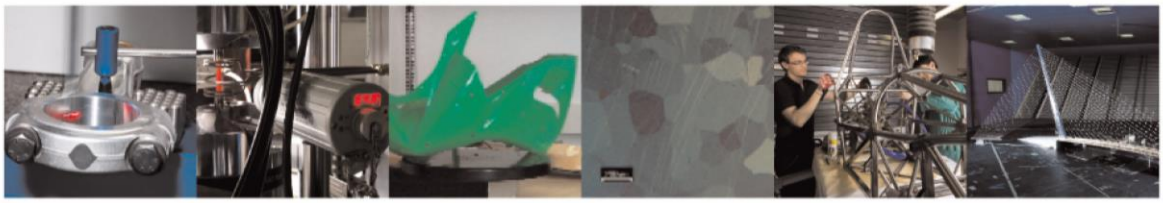

Surface morphology prediction model for milling operations

Torta, M.; Albertelli, P.; Monno, M.

DIPARTIMENTO DI MECCANICA ■ POLITECNICO DI MILANO
via G. La Masa, 1 ■ 20156 Milano ■ EMAIL (PEC): pecmecc@cert.polimi.it
http://www.mecc.polimi.it
Rev. 0

Int J Adv Manuf Technol manuscript No.
(will be inserted by the editor)

Surface morphology prediction model for milling operations

Mattia Torta · Paolo Albertelli · Michele Monno

Received: date / Accepted: date

Abstract The capability of estimating the surface quality of workpieces in machining is still a challenging goal. The morphology of the processed surfaces does not only depend on nominal tool geometry and on machining parameters but it is also affected by several complex cutting phenomena and deviations from nominal conditions. In this paper, a framework model for estimating the surface texture in milling operations was developed. The model allows considering various tool geometries and the corresponding alignment/mounting errors. Since the back cutting phenomenon is adequately formalized, the model is particularly suitable for estimating the surface topography in face milling. Although the model does not consider the contribution due to the cutting forces, it is suitable for being fed by measured tool vibrations. The predicting capabilities of the conceived model were tested considering a high-feed milling operation that typically generates complex patterns on the processed surfaces. The model validation was carried out comparing the numerical and the real machined surface morphology. The analysis confirmed that the surface morphology can be predicted with negligible errors.

Keywords Milling modelling · Machined surface morphology · Surface topography · Machining signature

M. Torta
Consorzio MUSP, strada Torre della Razza, 29122 Piacenza, Italy
Tel.: +39-0523-523190
Fax: +39-0523-645268
E-mail: mattia.torta@musp.net

P. Albertelli
Mechanical Engineering Department, Politecnico di Milano, via La Masa 1, 20156 Milan, Italy
E-mail: paolo.albertelli@polimi.it

M. Monno
Mechanical Engineering Department, Politecnico di Milano, via La Masa 1, 20156 Milan, Italy
E-mail: michele.monno@polimi.it

1 Introduction

In machining, the possibility of predicting the overall machine behaviour as well as the properties of the processed part in terms of geometrical errors, surface quality and surface morphology would be extremely useful for production engineers and machining experts that often rely, for selecting the machine, the tools and the process parameters, more on their expertise than on structured methodologies. This leads to the adoption of over-simplified approaches. In many high-value applications, the quality of the machined surfaces as well as the corresponding process signature are properties that affect the performance and the functionality of the processed component, [5, 10]. For this reason, from the manufacturing side, assuring the achievement of the desired outcomes is not a trivial task. Although the surface roughness Ra is the most widely adopted synthetic indicator for describing, especially in industry, the surface quality, often it is not suitable for performing adequate evaluations regarding the workpiece functionalities, [14, 15]. In recent years, since the availability of areal topography measuring instruments allows extending and enhancing the surface analysis capabilities [29], the research efforts towards the surface morphology prediction in machining processes have been increased.

According to the specific literature [5], various methodologies, each one with positive and negative aspects, were developed by researchers in order to predict the surface roughness. The first methodology is based on a physical model of the machining process, one relates on experimental approaches and lastly, techniques based on artificial intelligence can be exploited although they need experimental data from the field. Even the possibility of combining physical-based models with experimental data coming from the field (concept of cyber physical system *CPS*) seem the most promising recent trend, [19].

Focusing on milling, models that describe the interaction between the cutting edge and the workpiece have been matter of study since the mid '80s. When the tool is machining a work-part, according to its geometry, it generates a complex surface. For instance, if a cylindrical tool is considered, it generates a surface on its floor and a wall surface in correspondence to its side. If the generation of the side surface topography is relatively easy to be modeled and predicted since the interaction between the tool and the work-piece can be roughly studied in two dimensions (i.e. considering a series of cross-sections of the tool, perpendicular to its axis), the interaction between the bottom of the tool and the linked processed surface is much more difficult to be analyzed. Indeed, in such a case, a $3D$ approach is required.

For this reason, peripheral milling has been the most studied machining process. Elbestawi et al. [12] simulated the machined surface topography by taking into account the effect of cutting speed, immersion ratios, flank wear, tool vibration and run-out. For the prediction of the wall surface in peripheral milling, Ehmann and Hong [11] were the first authors that combined the machine tool kinematics model and the cutting tool geometry with the possibility to consider the machine vibrations. Lee et al. [20] included data from the field (tool vibrations estimated from acceleration measurements) in their model for the surface roughness prediction. The experimental validation showed quite good estimation capabilities although some limitations, in case of high-frequency vibrations, were observed. Xu et al. [30] developed a model for the

surface morphology in peripheral milling. They considered static and dynamic cutter deflection as well as the force on the tool. Relevant estimation errors were observed when high vibrations (unstable machining) were considered. A deep study of the effect of cutters runouts in peripheral milling is proposed by Schmitz et al. [28]. After a partial validation, the model was used for analyzing the effect of several parameters on surface roughness. Omar et al. [26] extended the previous model even taking into account the wear of the flank. The tool was axially discretized and for each cutting edge portion, the interaction with the meshed work-part was calculated for computing the resulting cutting force, [12]. The model was validated by a set of simulation runs and it seemed capable of predicting both the cutting force components as well as the surface topography of simple references cases found in literature. An extended validation, based on structured cutting tests, would have been useful for understanding the real capabilities of the modeling approach. Buj-Corral et al. [7] and Yang and Liu [31] studied the influence of different parameters on the surface topography in peripheral milling. If the first modelling approach seemed too simplified, the second research, after a proper validation, demonstrated, through simulations [17], that the deflection of the tool is the most influential parameter over the generated surface profile. The relevance of the cutting vibrations on the resulting machined surfaces was also studied by Jiang et al. [16], Arizmendi et al. [4] and Costes and Moreau [9].

For what concerns the floor topography face milling operations, in [23], a rather simple kinematic model of the milling process was considered and coupled with a cutting force model. The back cutting was even considered by Ryu et al. [27]. Another generalized model was developed by Altintas and Engin [2]. The profile of each cutting edge was parametrically described and its position was then computed ([24]) in order to calculate the chip thickness, the cutting forces and, as a consequence, the corresponding vibrations. In both the previous researches, the comparison with experiments revealed quite good predicting properties although the use of a too simplified dynamic modeling can affect the results in more complex test cases. Li et al. [21] simulated the floor surface topography in end mill exploiting a model based on the pure kinematics interaction between the inserts and the processed material. Recently, Muñoz-Escalona and Maropoulos [25] developed a geometrical model for surface roughness prediction in face milling with square inserts. Although the model did not considered some relevant aspects like cutting vibrations, tool deflection, and the back cutting effect, the simulations showed a quite good matching with the experimental roughness measurements. This is mainly due to the specific adopted validation test conditions. Much of the research carried out for predicting the floor surface refers to ball-end milling since it is typically used for finishing parts, [18, 6, 3, 8, 13]. Few works even dealt with $5-axis$ ball-end milling, [32, 22, 10]. Most of these researches focused on the macroscopic (scallop height evaluation) effect of the geometrical intersection between tool and the machined workpiece. Some of them studied the effects of cutting parameters but only in few of them a proper comparison between the predicted morphology and the observed one was carried out.

According to the performed literature analysis, in this research an innovative and generalized model for the topography prediction of the machined surfaces in milling operations was developed. More specifically, the model is suitable for predicting the surface morphology of both the wall and the floor of a generic milling operation.

The model is based on a geometric engine that considers the description of the tool geometry and the discretized representation of the piece. From the geometrical point of view, it considers the real insert geometry, including radial and axial run-out or mounting errors. The model takes into account the back cutting phenomenon and it is suitable for being fed by experimental measurements of the tool vibrations. In this paper, the predicting capabilities of the model were tested considering a high-feed face milling application in which, typically, due to the insert geometry and the machining parameters, the processed surfaces, created by the bottom part of the tool, exhibit very complex patterns. The validation of the model was carried out comparing the estimated $3-D$ surface morphology and the scanned one. The paper is structured as follows. In section 2 different aspects of the developed model were introduced. The formalism used for describing the tool kinematics and its geometrical modeling are presented in section 2.1. The tool-workpiece interaction is formalized in section 2.2. In section 3 the model validation procedure is described and the results are critically discussed in section 3.2.

Nomenclature

$\mathbf{0_1}$	Reference System
$\boldsymbol{I}$	Identity Matrix
$\boldsymbol{p}$	Vector describing the position of a generic point on the cutting edge with respect to reference system $\mathbf{0_1}$
$\boldsymbol{R}$	Rotation matrix
$\Delta\boldsymbol{p}$	Vector describing the relative position of the reference $\overline{\mathbf{0}}_\mathbf{2}$ with respect to framework $\mathbf{0_1}$
Δs	Discretization step of the curvilinear abscissa
Δt	Time interval for the simulation
$\Delta X, \Delta Y, \Delta Z$	elements of the vector $\Delta\boldsymbol{p}$
Δx_{1r}	mesh size ratio along x_1 direction
Δx_1	mesh size along x_1 direction
Δy_{1r}	mesh size ratio along y_1 direction
Δy_1	mesh size along y_1 direction
Δz_{1r}	mesh size ratio along z_1 direction
Δz_1	mesh size along z_1 direction
$\hat{x}_3, \hat{y}_3, \hat{z}_3$	Coordinates of the reference system $\hat{\mathbf{0}}_\mathbf{3}$
vib	Tool vibration
v	unit vector linked to the tool rotation axis
ω	Tool rotation velocity
$\overline{\mathbf{0}}_\mathbf{2}$	Reference System associated to the tool centre
$\overline{\boldsymbol{p}}$	Vector describing a generic position on the cutting edge with respect to reference $\overline{\mathbf{0}}_\mathbf{2}$
$\bar{x}_2, \bar{y}_2, \bar{z}_2$	Coordinates of the reference system $\overline{\mathbf{0}}_\mathbf{2}$
θ	Rotation angle
θ_e	Tool lead angle
$\widetilde{\mathbf{v}}$	cross-product matrix

a_e	Radial depth of cut
a_p	Axial depth of cut
D_{int}	Internal diameter of the tool
D_{nom}	Nominal diameter of the tool
f_j	Generic j^{th} component of the axis feed velocity
f_z	Feed per tooth
R	Tool radius
R_e	Insert tip radius
Ra	Surface roughness
s	curvilinear abscissa
t	time
t_i	Generic discretized i^{th} time instant
x_1, y_1, z_1	Coordinates of the reference system $\mathbf{0_1}$
Z	number of teeth

2 Material and Methods

In this section, the developed model for the estimation of the surface morphology in milling is presented. More specifically, both the process kinematics and the tool description are formalized. In addition, the tool-workpiece interaction engine is described.

2.1 Kinematic model of the milling process

Since the surface signature estimation, with the conceived approach, is provided by coupling the tool-workpiece geometrical interaction model together with a module for the tool motion description, a proper three-dimensional kinematic modelling of the tool is formalized. It was decided to analytically describe the profile of each cutting edge in terms of position and orientation when the tool is performing a general milling operation. It was done by defining a reference coordinate system and a series of subsequent transformations. Let us consider a generic fixed coordinate system $\mathbf{0_1} = \{0_1, x_1, y_1, z_1\}$ as the reference system. Each kinematic transformation describes the position and the orientation referred to a new reference system. The complex motion of a single cutting edge can be described as a rotation around a moving coordinate system $\overline{\mathbf{0}}_\mathbf{2} = \left\{\overline{0}_2, \overline{x}_2, \overline{y}_2, \overline{z}_2\right\}$. This coordinate reference system is shown in Figure 1 and it is based upon two main assumptions: the tool body and the cutting inserts (or cutting teeth) do not undergo any deformation or reciprocal displacement and the tool system motion $\overline{\mathbf{0}}_\mathbf{2}$ with respect to $\mathbf{0_1}$ is a pure translational motion without any rotation. Although this modelling approach allows an easy representation of the cutting edge nominal kinematics, it is not suitable for representing any bending deformation.

The position and the orientation of the tool are described by the coordinate system $\overline{\mathbf{0}}_\mathbf{2} = \left\{\overline{0}_2, \overline{x}_2, \overline{y}_2, \overline{z}_2\right\}$ with respect to the reference $\mathbf{0_1}$; this reference system is ideally fixed to the tool center, aligned with the machine axes and it moves according to the tool center position. Its description, with respect to the reference system, is defined

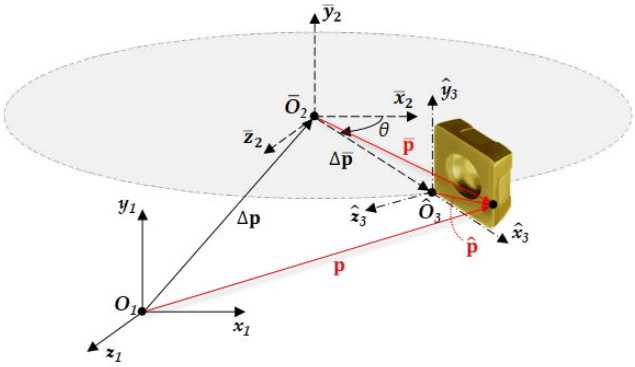

Fig. 1 reference kinematic framework

by pure transnational motion, Eq. 1:

$$\boldsymbol{p} = \overline{\boldsymbol{p}} + \Delta\boldsymbol{p} \tag{1}$$

Where $\overline{\boldsymbol{p}}$ is the vector that describes the position of a generic point on the cutting edge with respect to $\overline{\mathbf{0}}_\mathbf{2}$, and $\boldsymbol{p}$ is its representation with respect to $\mathbf{0_1}$. The transnational contribution is depicted in Fig. 1 and is defined as follows:

$$\Delta\boldsymbol{p} = \overrightarrow{0_1\bar{0}_2} = (\Delta X, \Delta Y, \Delta Z)^T \tag{2}$$

The cutting edge position and orientation are then defined by the coordinate system $\hat{\mathbf{0}}_\mathbf{3} = \left\{\hat{0}_3, \hat{x}_3, \hat{y}_3, \hat{z}_3\right\}$. In such reference system, the geometrical properties as well as the $3D$ configuration of the cutting edge can be defined. This modelling approach allows considering peculiar aspects (i.e. insert run-outs) and it is suitable for taking into account indexable cutters with inserts, as well as end-mills with complex cutting edge profiles. The coordinate reference system $\hat{\mathbf{0}}_\mathbf{3}$ integrally moves with the tooth/insert. Its motion is described with respect to the tool center coordinate system $\overline{\mathbf{0}}_\mathbf{2}$ and it can be formalized considering a combination of a translational contribution and a rotational contribution.

$$\bar{\mathbf{p}} = \boldsymbol{R}(\theta)\,\hat{\boldsymbol{p}} + \Delta\bar{\boldsymbol{p}} = \underbrace{\boldsymbol{R}(\theta)\,\hat{\boldsymbol{p}}}_{\left\{\hat{0}_3, \hat{x}_3, \hat{y}_3, \hat{z}_3\right\}} + \underbrace{\boldsymbol{R}(\theta)\,(R,0,0)^T}_{\overrightarrow{\bar{0}_2\hat{0}_3}} \tag{3}$$

Where $\bar{\mathbf{p}}$ is the representation of a point with respect to $\overline{\mathbf{0}}_\mathbf{2}$, R is the tool radius and $\boldsymbol{R}(\theta)$ is the rotation matrix in the following form:

$$\boldsymbol{R}(\theta) = \mathbf{I} + \tilde{\mathbf{v}}\sin\theta + 2\tilde{\mathbf{v}}^2\sin^2\frac{\theta}{2} \tag{4}$$

where $\boldsymbol{I}$ is the identity matrix and $\tilde{\mathbf{v}}$ the $cross-product$ matrix for the unit vector $\mathbf{v} = (v'_x, v'_y, v'_z)$ that represents the axis of rotation.

$$\widetilde{\mathbf{v}} = \begin{bmatrix} 0 & -v'_z & -v'_y \\ v'_z & 0 & -v'_x \\ -v'_y & v'_x & 0 \end{bmatrix} \tag{5}$$

This is the so-called *Rodriguez's* formula for the rotation matrix, expressed in terms of the angle of rotation θ. At this point, it is rather simple to describe the position of $\hat{\mathbf{p}}$ with respect to the reference system:

$$\mathbf{p} = \mathbf{R}(\theta)\,\hat{\mathbf{p}} + \mathbf{R}(\theta)\,(R,0,0)^T + \Delta\mathbf{p} \tag{6}$$

From Eq. 6, the contribution of tool center vibrations may be introduced by adding a translational contribution $\Delta\mathbf{vib}$ that represents the vibration of $\bar{\mathbf{0}}$ with respecto to $\mathbf{0}$ (tool tip oscillation) due to the machined flexibility, so that:

$$\mathbf{p} = \mathbf{R}(\theta)\,\hat{\mathbf{p}} + \mathbf{R}(\theta)\,(R,0,0)^T + \Delta\mathbf{p} + \Delta\mathbf{vib} \tag{7}$$

As previously described, in the model formulation it was decided to take into consideration the contributions linked to the machine vibrations $\Delta\mathbf{vib}$ through the tool tip oscillation measurements that can be carried out with a specific laboratory setting or using an estimation approach based on Kalman Filter as developed in Albertelli et al. [1]. Time dependency is finally introduced considering $\theta = \omega\, t$ with ω representing the actual spindle speed and $\Delta\mathbf{p} = (f_x t, f_y t, f_z t)^T$ where f_j represents the generic j^{th} component of the feed velocity vector. This discrete time evolution is based upon a time interval Δt so that $t_{i+1} = t_i + \Delta t$.

2.2 Tool-workpiece interaction model

So far, the overall cutting edge motion has been modeled with respect to a fixed reference system. However, in order to get a realistic representation of the surface signature, a proper tool-workpiece interaction model was created. For sake of generality, the developed approach is suitable for being used with any cutting tool geometry but, in order to be more effectively presented, a high feed milling indexable tool cutter was taken as the reference case, Fig. 2. As can be easily noted in Fig. 2, the red line, that is the portion of the cutting edge potentially involved in the cut, is defined with respect to the local coordinate system $\hat{\mathbf{0}}_\mathbf{3}$. Referring to the specific case, the active cutting edge portion is composed by the circular arc $\widehat{AB}$ and the linear segments $\overline{BC}$ and $\overline{CD}$. It is clear how any other cutting edge profile can be similarly defined.

The idea that underpins the proposed approach is the discretization of the workpiece volume in two subsequent steps. At first, the volume is subdivided into two-dimensional slices parallel to the feed direction x_1. The overall number of slices and the step between them define the discretization approach used along the transversal direction z_1. The second discretization step is carried out by meshing each slice with a predetermined resolution both along feed (x_1) and axial (y_1) directions. This twofold discretization procedure is described in Fig. 3, where the interaction between the tool and a generic slice of processed material is also illustrated. The discretization resolution affects both the simulation results and the computational time. Depending on

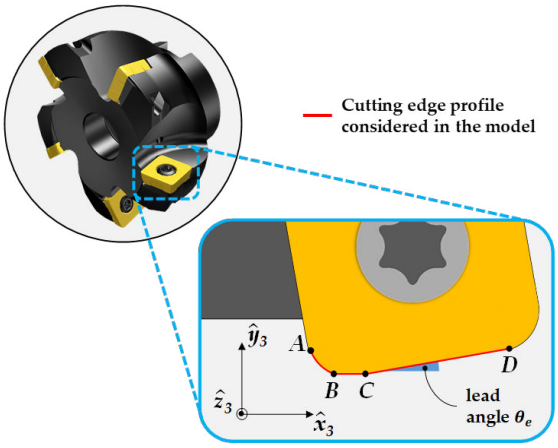

Fig. 2 reference kinematic framework

the simulated milling operation, the most appropriate mesh sizes compromise need to be found. Surely, an equal sub-micrometric discretization mesh, accross all the considered directions (x_1, y_1, z_1), would satisfy the accuracy specification but, at the same time, it would result in an infeasible simulations time. For this reason, a specific meshing size has to be selected for each direction. According to the accomplished expertise, the following rough guidelines can be taken into account for the first mesh selection without considering tool vibrations: $\Delta x_{1r} = 1/10 - 1/100$ of the f_z along x_1, $\Delta y_{1r} = 1/10 - 1/50$ of the expected floor surface roughness Ra along y_1 and $\Delta z_{1r} = 1/5 - 1/20$ of the expected side roughness Ra along z_1.

The roto-translational tool motion drives each cutting edge through the slice leaving subsequent traces of the edge profile.

The combination of each subsequent edge trace on a slice defines a relative $2D$ surface profile; by combining each slice involved in the cutting process, the 3D surface topography can be obtained. The intersection between each cutting edge and the involved slices is a critical part of the tool-workpiece interaction model. Once the workpiece has been discretized, two main aspects need to be considered. Firstly, the cutting edge portion involved in the process needs a discrete representation in order to properly interact with the workpiece. Secondly, since the tool motion is also time-discrete, a proper representation of the edge position in-between the positions corresponding to two subsequent time instants is mandatory in order to model how the cutting edge crosses each slice. These aspects have been tackled by the discretization and intersection approach represented in Fig. 3 and 4.

The geometrical description of the cutting edge profile was done considering a curvilinear abscissa s so that:

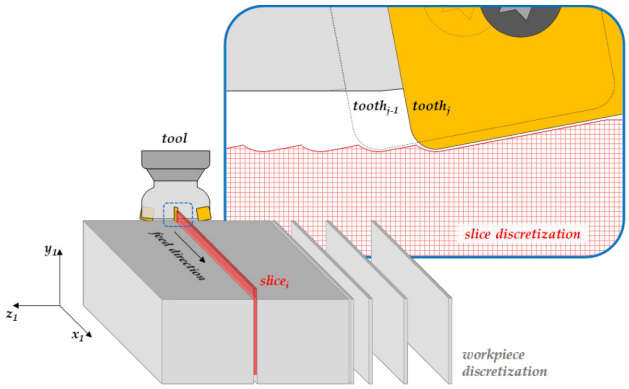

Fig. 3 Workpiece discretization process by slicing along feed direction. Discretization process used to approximate and collect the subsequent cutting edge traces

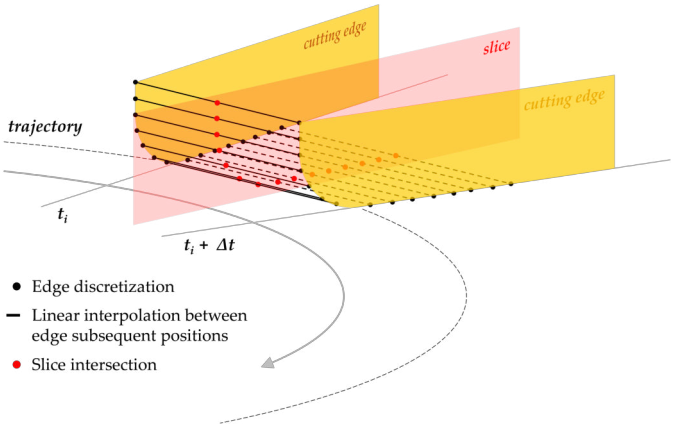

Fig. 4 Slice intersection process. The actual edge profile is geometrically described and then discretized (black dots); the discretization points of two subsequent edges are then linearly interpolated (black solid lines) and the intersection point on the slice plane are then identified (red dots)

$$\begin{cases} \hat{x}_3(s) = \begin{cases} R_e \sin\left(\frac{s}{R_e}\right) & A < s < B \\ R_e + s - \frac{\pi R_e}{2} & B < s < C \\ R_e + \overline{BC} + \left(s - \overline{BC} - \frac{\pi R_e}{2}\right)\cos\theta_e & C < s < D \end{cases} \\ \hat{y}_3(s) = \begin{cases} R_e\left[1 - \sin\left(\frac{s}{R_e}\right)\right] & A < s < B \\ 0 & B < s < C \\ \left(s - \overline{BC} - \frac{\pi R_e}{2}\right)\sin\theta_e & C < s < D \end{cases} \\ \hat{z}_3(s) = 0 \end{cases} \tag{8}$$

Where θ_e is the lead angle of the insert as represented in Fig. 2, and R_e represents the radius of the portion $\widehat{AB}$. The edge so represented can be discretized along the

curvilinear coordinate using a step Δs. Once the edge has been discretized, the conceived tool-workpiece interaction approach can be finally introduced. Since a perfect alignment between a generic edge position and the slice being crossed is quite unlikely, the proposed approach takes into account two subsequent edge position and the linear interpolation between them. Moreover, as represented in Fig. 4, the linear interpolation is made for all the points (along s) of the edge portion involved in the cut. More precisely, this interpolation was performed considering each couple of discretization points belonging respectively to the edge at time t_i and its corresponding position at time $t_i + \Delta t$. The so defined linear segments intersect the slice and generate a series of intersection points, represented in Fig. 4 as red dots. These points lie onto the slice plane and represent a discretized trace left by the cutting edge when it crosses the slice. In order to find the coordinates of these intersection points, the equations reported in Eq. 9 were used. They refer to the the tridimensional representation of a two-point linear segment.

$$\frac{x_1 - x_{1,0}}{x_{1,1} - x_{1,0}} = \frac{y_1 - y_{1,0}}{y_{1,1} - y_{1,0}} = \frac{z_1 - z_{1,0}}{z_{1,1} - z_{1,0}} \tag{9}$$

To find where this segment intersects the slice plane, the plane equation $x_{3,slice} = \bar{x}_3$ must be introduced into the system:

$$\begin{cases} \frac{x_1 - x_{1,0}}{x_{1,1} - x_{1,0}} = \frac{z_1 - z_{1,0}}{z_{1,1} - z_{1,0}} \\ \frac{y_1 - y_{1,0}}{y_{1,1} - y_{1,0}} = \frac{z_1 - z_{1,0}}{z_{1,1} - z_{1,0}} \\ z_1 = \bar{z}_2 \end{cases} \tag{10}$$

And rearranging the equation, the following relationships can be obtained in order to extract the coordinates of the intersection points:

$$\begin{cases} x_1 = \frac{\bar{z}_2 - z_{1,0}}{z_{1,1} - z_{1,0}} (x_{1,1} - x_{1,0}) + x_{1,0} \\ y_1 = \frac{\bar{z}_2 - z_{1,0}}{z_{1,1} - z_{1,0}} (y_{1,1} - y_{1,0}) + y_{1,0} \\ z_1 = \bar{z}_2 \end{cases} \tag{11}$$

The identified cutting edge profile, as the results of the intersection process, undergoes a resampling operation in order to adapt its geometry to the slice discretization grid. After that, the portion of the slice representing the material being cut is removed from the mesh. As already described, for a generic slice, the edge portion involved in the cut may not be the whole edge profile. For each time instant, the portion that actually crosses a certain slice depends on a series of aspects. For instance, the slice position and orientation with respect to the tool center, the cutting edge geometry, the cutting tool configuration and so on. In order to account for a proper interaction, the approach must ensure the correct selection of this cutting edge portion. This task is carried out by taking into account all the possible edge-slice relative configuration and by accordingly identifying the edge portion involved in the cut. This process is shown, just for some noteworthy cases, in Fig. 5. Points A and D respectively represents the cutting edge starting and ending points (as in Fig. 2). The red line corresponds to the workpiece slice being considered, P_t and P_t' are the edge discretization points nearest to the slice and the light red area is connected to the trace

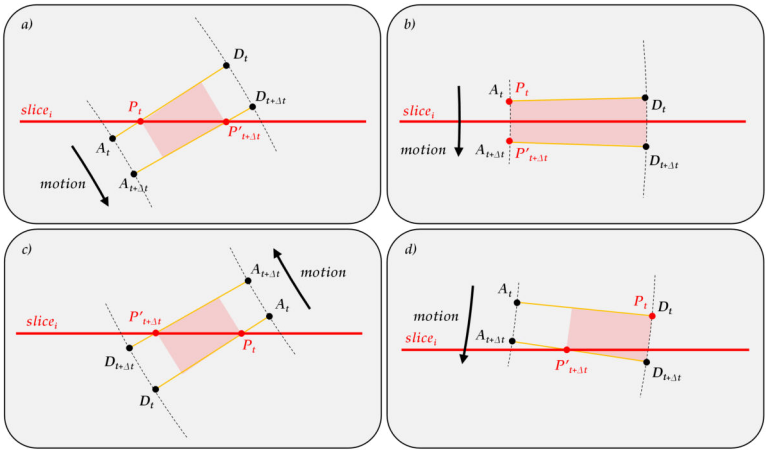

Fig. 5 Some example of the intersection process in a 2*D* view. (a) front cut case with double intersection, (b) front cut case with no slice intersection, (c) back cut case with double slice intersection, (d) front cut case with single slice intersection

of the cutting edge portion involved in the cut. Fig. 5(a) depicts a slice being crossed in a front cut case by a portion of the cutting edge. Considering the generic time t_i and the following time instant $t_i + \Delta t$, the involved edge portion starts at P_t and ends at $P'_{t+\Delta t}$ since these are the points of the cutting edge nearest to the workpiece slice in such instants. A peculiar case is shown in Fig. 5(b), where the slice being considered is crossed without any intersections. In such cases, when $P_t = A_t$ and $P'_{t+\Delta t} = A_{t+\Delta t}$, the whole cutting edge is considered involved in the cut. Furthermore, a generic slice is crossed in a back cut case in Fig. 5(c). Here, the applied approach is similar to what done in Fig. 5(a) and the involved cutting edge portion is identified accordingly. Lastly, Fig. 5(d) depicts a case where the edge-slice intersection results only for one of the two represented subsequent cutting edge positions. In such a case, one of the boundary points (P_t in this case) corresponds to either point A or point D (D_t in this case).

It is worth of remarking that the conceived modelling approach is generic and it allows to deal with several milling operations ranging from face milling to contouring, even considering up and down-milling. Indeed, the approaches used for the workpiece discretization and for the workpiece-tool interaction fit with a generic milling operation. Even in the case of adopting tools with a complex geometry (i.e. end-mill, ball-end mill, etc.) instead of indexable cutters, the model can be easily adapted reformulating Eq. 8.

The overall simulation model comprising the kinematic and the interaction part is the implemented in a *MATLAB* environment on a 64 *bit* platform equipped with an Intel Core $i7-3740QM$ processor and 8 *GB* of *RAM*.

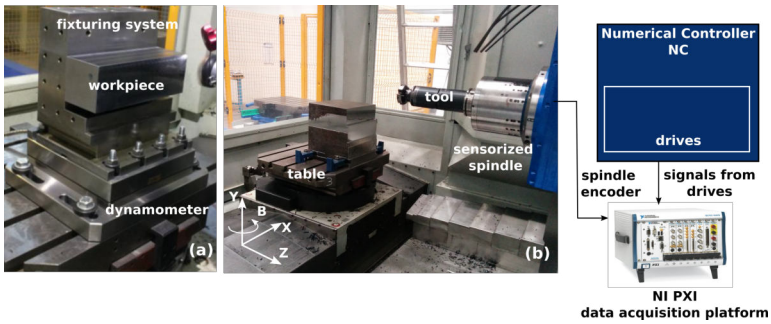

Fig. 6 Processed workpiece (a), adopted machine and acquisition systems (b)

3 Results and Discussion

In order to validate the overall simulation approach, a real cutting test was performed. The morphology of the machined surface was compared to the simulated results and they were discussed in Section 3.2. Since the literature is rather poor of models suitable for reproducing face milling operations, in this research it was decided to focus on a high-feed tool that is typically used for facing in many fields (i.e. mold and dies production). More details on the used machine tool, the experimental set-up, the adopted cutting parameters and the instrumentation are reported in Section 3.1.

3.1 Experimental set-up

The cutting test was executed with a $4-axis$ machine tool (*Mandelli M5*), Fig. 6 (b). The machine is equipped with an electro-spindle that can provide up to $160\,Nm$ and can reach the maximum rotational speed of $8000\,rpm$. The machine was equipped with an acquisition system from *National Instruments* in order to get the data related to the spindle position and feed velocity during the experiments (rotation angle θ and feed axis velocity f_j). The milling test was executed on a $C45$ steel workpiece that was specifically designed for being hold with the fixturing system depicted in Fig. 6 (a).

A commercial high-feed tool with the nominal diameter of $D_{nom} = 80\,mm$ and $Z = 6$ teeth, from *Sandvik Coromant*, was adopted for the cutting test. Commercial codes of both the tool body and the cutting inserts were reported in Table 1. The first rough modelling of the tool was reported in Fig. 2. In order to improve the accuracy of the morphology prediction, a better representation of the tool geometry was developed by taking into account the axial run-out of each insert. In order to characterize them, specific measurements with a comparator gauge were executed. The maximum measured value was $24\,\mu m$. The effect of run-out was then introduced in the simulation model by applying a translational contribution to the cutting edges along the $\hat{x}_2$ direction. As a results of such a precise characterization, the insert geometry used in the simulation is reported in Fig. 7. For the analyzed test case, the mesh sizes

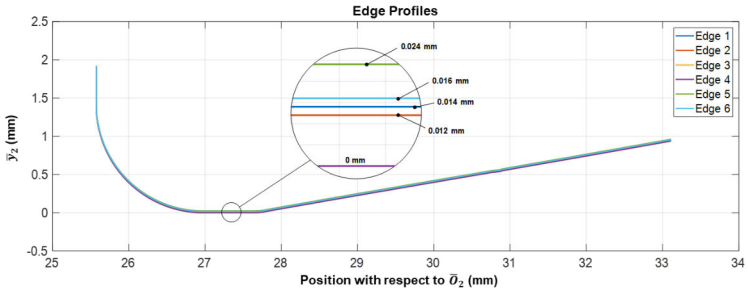

Fig. 7 Modelled insert geometry. Edge 3 and edge 4 have the same value of axial runout.

$(\Delta x_1, \Delta y_1, \Delta z_1)$ reported in Table 1 were adopted. They agree with the guidelines previously presented.

For what concerns the cutting parameters selection, they were reported in Table 1. Although the developed model is suitable for being fed with vibration data coming from the field (i.e. from a non-contact displacement sensor placed close to the tool tip or estimating the tool vibration Albertelli et al. [1] from other measurements), in this paper they were not considered. Indeed, in order to avoid excessive tool vibrations , very conservative cutting parameters were chosen, Table 1. The test is conducted in slot-milling configuration ($a_e \simeq D_{int}$).

For being able to compare the simulated morphology and the real machined surface, the latter was scanned with a white light interferometer provided by *Mahr* (*MarSurf CWM* 100). A specific camera form *Allied Vision* (*Prosilica GT* 2300) and a lighting system based on 4 *LED* bars and 1 *LED* ring, both from *CCS*, were used for creating the surface pictures. The comparison was not done only from a qualitative point of view but even comparing the numerical and measured resulted profiles, section 3.2.

Parameter	Value	Unit
Tool Code	$R210-080Q27-14H$	–
Insert	$R210-14\ 05\ 14E-PM$ 1030	–
Insert tip radius R_e	1.4	mm
Internal tool diameter D_{int}	56	mm
External tool diameter D_{nom}	80	mm
Cutting edge lead angle θ_e	10	deg
Cutting inserts	6	–
Feed per tooth f_z	1	$mm/(tooth \cdot rev)$
Axial depth of cut a_p	0.6	mm
Radial depth of cut a_e	$\simeq D_{int}$	mm
Spindle speed	970	rpm
Simulation time step	2e-4	s
Discretization step Δx_1	10	μm
Discretization step Δy_1	0.1	μm
Discretization step Δz_1	10	μm
Cutting edge discretization step Δs	100	μm

Table 1 Experimental cutting coefficients identification

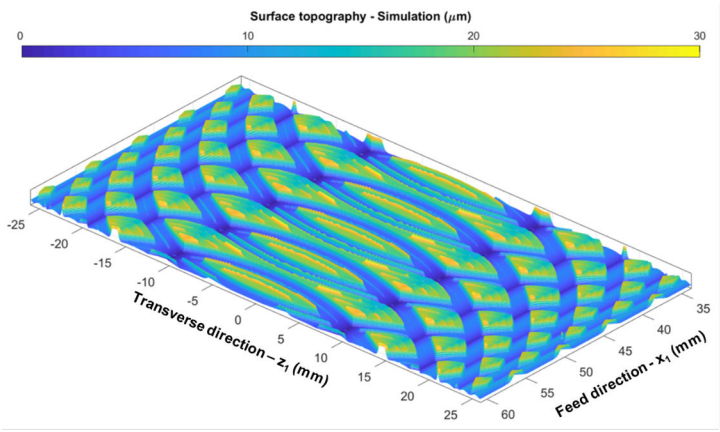

Fig. 8 Simulated 3D surface topography

3.2 Model Validation and results discussion

The simulation results are reported in Fig. 8, where the whole surface is represented and the topography characteristics can be observed; the simulation took 3.5 h to be completed. In order to improve the predicting capabilities of the model, the simulations were performed considering the real machine tool kinematics (f_j) and the tool rotation angle θ, both measured through the acquisition system from *NI PXI* (Fig. 6) during the experimental test. In Fig. 9, the comparison between the real manufactured surface (both capturing a picture (top) and as the result of a scanning operation (bottom)) and the simulated one (middle) in the same scale and from the same perspective is underlined.

The simulated results (Fig. 9 (middle)) show an interesting interlaced pattern reproduction that thickens from the center to the peripheral part and a good representation of both the floor and the peripheral surface. This promising results are ensured also by modeling the interaction between front cut and back cut traces. However, it is worth pointing out that the chip generation phenomenon is not considered since the interaction between the cutting edge and the workpiece is a pure volume subtraction. The simulated surface shows also the peculiar run-out effect, identified by a two-to-six periodic cycloidal trace left for both front and back cutting. This trace is clearly below the ones related to other cutting edges, due to the axial position of edge 3 and 4 with respect to the others. Looking at Fig. 9, patterns similarities can be appreciated. The model is able to reproduce the complex cycloidal patterns that define the surface topography. The geometrical structures and their spatial features are well estimated; the large interlacement in the middle of the surface, where the rotational curvature is minimum, can also be observed in the machined surface. Likewise, the simulated runout effect matches quite well the counterpart on the real surface; the periodicity as well as the spatial characteristics involved find a proper reproduction. Actually, some minor discrepancies can be observed. For instance, the simulated surface shows that all the insert marks seem to have the same depth along y_1 axis while in the re-

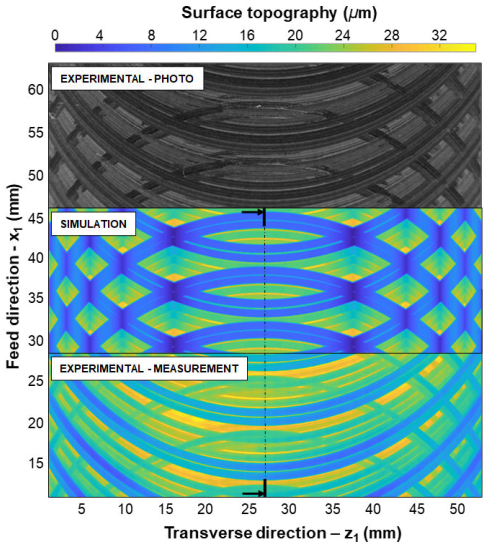

Fig. 9 Comparison between the simulated surface topography (middle) and the real machined surface (top) and scanned with the interferometer (bottom)

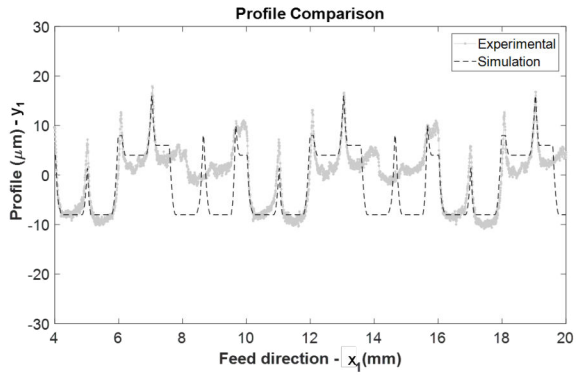

Fig. 10 Simulated-measured profile comparison - cross-section obtained from Fig. 9

ported experimental results the back-cut action of the inserts seems having made less visible marks. This is most likely due to the tool bending deflection caused by the average cutting forces that acted along the feed axis x_1. This aspect, together with, the tool vibrations were not considered in this research. Anyway, an acceptable overall matching between the numerical and the experimental results is even confirmed by focusing on Fig. 10, where the profiles, obtained with a cross-section along the center-line ($z_1 = 28$ *mm*) parallel to the feed direction, of the simulated surface morphology and the scanned one are compared. A better visualization of the previously described mismatch can be appreciated in the cross-section (i.e. form $x_1 = 7.8 - 9.8$ *mm*). Another phenomenon that could have affected the mismatch is the spring back

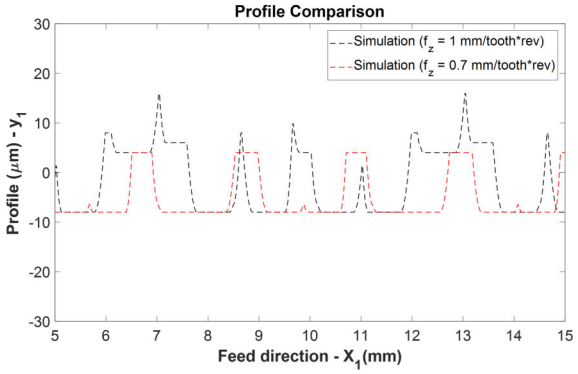

Fig. 11 Simulated profiles - the f_z effect

effect of the material being cut, which may elastically returns and thus undergoes a back cut. Even this aspect was not introduced in the developed model. Although these small discrepancies, the developed modelling approach seems a promising and powerful tool for predicting the processed surface textures in milling operations. In order to demonstrate the potentialities of the developed modelling approach, some simulations changing the feed rates were carried out. The obtained results are reported in Fig. 11. It can be seen that adopting a lower f_z, the irregularities due to the insert run-out (Fig. 11) are less visible. Simulations changing even other parameters could be carried out.

4 Conclusions and Future Works

A model for the prediction of the $3D$ surface topography in milling has been developed. The model is suitable for being fed by real cutting vibrations; also, different geometries and tool configurations can be considered. Front and back cutting can be modelled. A validation was carried out even considering the comparison between the simulated surface topography and the real counterpart, showing rather good reproduction capabilities. The experimental surface characterization was done using a $3D$ scanning system (white-light interferometer). Some other aspects will be studied in order to bridge the gap of the actual version of the model. Indeed, a deep assessment of prediction capabilities will be carried out for different kinds of material, trying also to take into account the material behavior with, for example, the spring-back effect. Secondly, a specific procedure will be developed in order to measure the actual position and shape of each cutting edge, allowing for a very accurate geometrical reproduction of the surface (taking into account, for example, the actual tool wear). Likewise, the efforts will be focused on the optimization of the algorithm in order to reduce the simulation time even though the idea is to get a surface representation at the end of the cutting process and not in a real-time fashion.

Acknowledgements This work was supported by the regional project SENSE&MILL 803442 (POR-FESR 2014-2020, Regione Emilia Romagna) and the national project CLUSTER La fabbrica Intelligente High Performance Manufacturing (*CTN*0100163216758), founded by MIUR.

References

1. Albertelli P, Goletti M, Torta M, Salehi M, Monno M (2016) Model-based broadband estimation of cutting forces and tool vibration in milling through in-process indirect multiple-sensors measurements. International Journal of Advanced Manufacturing Technology 82(5-8), DOI 10.1007/s00170-015-7402-x
2. Altintas Y, Engin S (2001) Generalized Modeling of Mechanics and Dynamics of Milling Cutters. CIRP Annals 50(1):25–30, DOI 10.1016/S0007-8506(07)62063-0, URL https://www.sciencedirect.com/science/article/pii/S0007850607620630
3. Antoniadis A, Savakis C, Bilalis N, Balouktsis A (2003) Prediction of Surface Topomorphy and Roughness in Ball-End Milling. The International Journal of Advanced Manufacturing Technology 21(12):965–971, DOI 10.1007/s00170-002-1418-8, URL http://link.springer.com/10.1007/s00170-002-1418-8
4. Arizmendi M, Campa F, Fernández J, López de Lacalle L, Gil A, Bilbao E, Veiga F, Lamikiz A (2009) Model for surface topography prediction in peripheral milling considering tool vibration. CIRP Annals 58(1):93–96, DOI 10.1016/J.CIRP.2009.03.084, URL https://www.sciencedirect.com/science/article/pii/S0007850609000377
5. Benardos P, Vosniakos GC (2003) Predicting surface roughness in machining: a review. International Journal of Machine Tools and Manufacture 43(8):833–844, DOI 10.1016/S0890-6955(03)00059-2, URL https://www.sciencedirect.com/science/article/pii/S0890695503000592
6. Bouzakis KD, Aichouh P, Efstathiou K (2003) Determination of the chip geometry, cutting force and roughness in free form surfaces finishing milling, with ball end tools. International Journal of Machine Tools and Manufacture 43(5):499–514, DOI 10.1016/S0890-6955(02)00265-1, URL https://www.sciencedirect.com/science/article/pii/S0890695502002651
7. Buj-Corral I, Vivancos-Calvet J, González-Rojas H (2011) Influence of feed, eccentricity and helix angle on topography obtained in side milling processes. International Journal of Machine Tools and Manufacture 51(12):889–897, DOI 10.1016/j.ijmachtools.2011.08.001, URL https://www.sciencedirect.com/science/article/pii/S0890695511001398
8. Chen JS, Huang YK, Chen MS (2005) A study of the surface scallop generating mechanism in the ball-end milling process. International Journal of Machine Tools and Manufacture 45(9):1077–1084, DOI 10.1016/J.IJMACHTOOLS.2004.11.019, URL https://www.sciencedirect.com/science/article/pii/S0890695504003050
9. Costes JP, Moreau V (2011) Surface roughness prediction in milling based on tool displacements. Journal of Manufacturing Processes 13(2):133–140, DOI 10.1016/j.jmapro.2011.02.003, URL https://www.sciencedirect.com/science/article/pii/S1526612511000089

10. Denkena B, Böß V, Nespor D, Gilge P, Hohenstein S, Seume J (2015) Prediction of the 3D Surface Topography after Ball End Milling and its Influence on Aerodynamics. Procedia CIRP 31:221–227, DOI 10.1016/J.PROCIR.2015.03.049, URL https://www.sciencedirect.com/science/article/pii/S2212827115002474
11. Ehmann K, Hong M (1994) A Generalized Model of the Surface Generation Process in Metal Cutting. CIRP Annals 43(1):483–486, DOI 10.1016/S0007-8506(07)62258-6, URL https://www.sciencedirect.com/science/article/pii/S0007850607622586
12. Elbestawi M, Ismail F, Yuen K (1994) Surface topography characterization in finish milling. International Journal of Machine Tools and Manufacture 34(2):245–255, DOI 10.1016/0890-6955(94)90104-X, URL https://www.sciencedirect.com/science/article/pii/089069559490104X
13. Gao T, Zhang W, Qiu K, Wan M (2006) Numerical Simulation of Machined Surface Topography and Roughness in Milling Process. Journal of Manufacturing Science and Engineering 128(1):96, DOI 10.1115/1.2123047, URL http://manufacturingscience.asmedigitalcollection.asme.org/article.aspx?articleid=1450271
14. ISO (2009) 4287 geometrical product specification (gps). surface texture: Profile method. terms, definitions and surface texture parameters. URL https://bsol.bsigroup.com/Bibliographic/BibliographicInfoData/000000000030167230
15. ISO (2012) https://bsol.bsigroup.com/search/search?searchkey=25178-2&originpage=header+search+box&autosuggestion=false. URL https://bsol.bsigroup.com/Bibliographic/BibliographicInfoData/000000000030154352
16. Jiang H, Long X, Meng G (2008) Study of the correlation between surface generation and cutting vibrations in peripheral milling. Journal of Materials Processing Technology 208(1-3):229–238, DOI 10.1016/J.JMATPROTEC.2007.12.127, URL https://www.sciencedirect.com/science/article/pii/S0924013608000381
17. Kline WA, DeVor RE, Shareef IA (1982) The Prediction of Surface Accuracy in End Milling. Journal of Engineering for Industry 104(3):272–278, URL http://dx.doi.org/10.1115/1.3185830
18. Lazoglu I (2003) Sculpture surface machining: a generalized model of ball-end milling force system. International Journal of Machine Tools and Manufacture 43(5):453–462, DOI 10.1016/S0890-6955(02)00302-4, URL https://www.sciencedirect.com/science/article/pii/S0890695502003024
19. Lee J, Bagheri B, Kao HA (2015) A Cyber-Physical Systems architecture for Industry 4.0-based manufacturing systems. Manufacturing Letters 3:18–23, DOI 10.1016/j.mfglet.2014.12.001, URL http://dx.doi.org/10.1016/j.mfglet.2014.12.001, 1503.07717
20. Lee KY, Kang MC, Jeong YH, Lee DW, Kim JS (2001) Simulation of surface roughness and profile in high-speed end milling. Journal of Materials Processing Technology 113(1-3):410–415, DOI 10.1016/S0924-0136(01)00697-5, URL https://www.sciencedirect.com/science/article/pii/S0924013601006975
21. Li S, Liu R, Zhang A (2002) Study on an end milling generation surface model and simulation taking into account of the main axle's tolerance. Journal of Materials Processing Technology 129(1-3):86–90, DOI 10.1016/S0924-0136(02)00581-2, URL https://www.sciencedirect.com/science/article/pii/S0924013602005812

22. Liu X, Soshi M, Sahasrabudhe A, Yamazaki K, Mori M (2006) A Geometrical Simulation System of Ball End Finish Milling Process and Its Application for the Prediction of Surface Micro Features. Journal of Manufacturing Science and Engineering 128(1):74, DOI 10.1115/1.2039098, URL http://manufacturingscience.asmedigitalcollection.asme.org/article.aspx?articleid=1450253
23. Melkote SN, Sutherland JW, King C (1999) The Effect of Tool Flexibility on Back-Cutting in End Milled Surfaces. Journal of Manufacturing Science and Engineering 121(3):532, DOI 10.1115/1.2832713, URL http://manufacturingscience.asmedigitalcollection.asme.org/article.aspx?articleid=1434817
24. Montgomery D, Altintas Y (1991) Mechanism of Cutting Force and Surface Generation in Dynamic Milling. Journal of Engineering for Industry 113(2):160–168, URL http://dx.doi.org/10.1115/1.2899673
25. Muñoz-Escalona P, Maropoulos PG (2015) A geometrical model for surface roughness prediction when face milling Al 7075-T7351 with square insert tools. Journal of Manufacturing Systems 36:216–223, DOI 10.1016/J.JMSY.2014.06.011, URL https://www.sciencedirect.com/science/article/pii/S0278612514000776
26. Omar O, El-Wardany T, Ng E, Elbestawi M (2007) An improved cutting force and surface topography prediction model in end milling. International Journal of Machine Tools and Manufacture 47(7-8):1263–1275, DOI 10.1016/J.IJMACHTOOLS.2006.08.021, URL https://www.sciencedirect.com/science/article/pii/S0890695506002136
27. Ryu SH, Choi DK, Chu CN (2006) Roughness and texture generation on end milled surfaces. International Journal of Machine Tools and Manufacture 46(3-4):404–412, DOI 10.1016/J.IJMACHTOOLS.2005.05.010, URL https://www.sciencedirect.com/science/article/pii/S0890695505001239
28. Schmitz TL, Couey J, Marsh E, Mauntler N, Hughes D (2007) Runout effects in milling: Surface finish, surface location error, and stability. International Journal of Machine Tools and Manufacture 47(5):841–851, DOI 10.1016/J.IJMACHTOOLS.2006.06.014, URL https://www.sciencedirect.com/science/article/pii/S0890695506001672
29. Townsend A, Senin N, Blunt L, Leach R, Taylor J (2016) Surface texture metrology for metal additive manufacturing: a review. Precision Engineering 46:34 – 47, DOI https://doi.org/10.1016/j.precisioneng.2016.06.001, URL http://www.sciencedirect.com/science/article/pii/S0141635916300721
30. Xu AP, Qu YX, Zhang DW, Huang T (2003) Simulation and experimental investigation of the end milling process considering the cutter flexibility. International Journal of Machine Tools and Manufacture 43(3):283–292, DOI 10.1016/S0890-6955(02)00213-4, URL https://www.sciencedirect.com/science/article/pii/S0890695502002134
31. Yang D, Liu Z (2015) Surface plastic deformation and surface topography prediction in peripheral milling with variable pitch end mill. International Journal of Machine Tools and Manufacture 91:43–53, DOI 10.1016/J.IJMACHTOOLS.2014.11.009, URL https://www.sciencedirect.com/science/article/pii/S089069551440021X

32. Zhang WH, Tan G, Wan M, Gao T, Bassir DH (2008) A New Algorithm for the Numerical Simulation of Machined Surface Topography in Multiaxis Ball-End Milling. Journal of Manufacturing Science and Engineering 130(1):011003, DOI 10.1115/1.2815337, URL http://manufacturingscience.asmedigitalcollection.asme.org/article.aspx?articleid=1451998